# Effects of postdeposition heat treatment on the structural and magnetic properties of $CoFe_2O_4$ nanoparticles produced by pulsed laser deposition

F. Fabris, , Y. T. Xing, , D. F. Franceschini, , D. R. Sanchez, , M. Alzamora, and , and W. C. Nunes

Citation: Journal of Applied Physics **122**, 063901 (2017); doi: 10.1063/1.4985789
View online: http://dx.doi.org/10.1063/1.4985789
View Table of Contents: http://aip.scitation.org/toc/jap/122/6
Published by the American Institute of Physics

# Effects of postdeposition heat treatment on the structural and magnetic properties of $CoFe_2O_4$ nanoparticles produced by pulsed laser deposition

F. Fabris,[1,a)] Y. T. Xing,[1] D. F. Franceschini,[1] D. R. Sanchez,[1] M. Alzamora,[2] and W. C. Nunes[1,b)]
[1]*Instituto de Física, Universidade Federal Fluminense, 24210-346 Niterói, Rio de Janeiro, Brazil*
[2]*Universidade Federal do Rio de Janeiro, 25245-390 Duque de Caxias, Rio de Janeiro, Brazil*

(Received 31 May 2017; accepted 26 July 2017; published online 9 August 2017)

In this work, we investigated the effects of postdeposition heat treatment on structural and magnetic properties of $CoFe_2O_4$ nanoparticles produced by pulsed laser deposition. Structural analysis by X-ray diffraction, transmission electron microscopy (TEM) and Mössbauer spectroscopy indicate the formation of a single phase cobalt ferrite nanoparticles with the size ranging from 4.3 to 33.3 nm depending on the annealing temperature. The magnetic properties of the samples were investigated in a wide temperature range (50–400 K). Noticeable effects of the cubic magnetocrystalline anisotropy on the magnetization process of nanoparticles were observed for samples annealed at 450 °C and 600 °C, while for samples as-deposited and annealed at 300 °C the magnetization properties were dominated by a uniaxial effective anisotropy. $\Delta M$ technique was used to investigate the magnetic interaction among the nanoparticles. Only demagnetizing interactions were observed for the sample annealed up to 300 °C, while for the samples treated at 450 °C and 600 °C, both magnetizing and demagnetizing interactions were observed. The results are discussed considering the evolution of the nanoparticles' nanostructure with anneals and its effects on the magnetic properties. *Published by AIP Publishing*. [http://dx.doi.org/10.1063/1.4985789]

## I. INTRODUCTION

Magnetic nanoparticles have been subject of extensive research over the last few decades. These systems exhibit unique nanoscale properties that offer several opportunities in industrial application, as well as in scientific research.[1,2] Particularly, cobalt ferrite $CoFe_2O_4$ (CFO) nanoparticles with a cubic spinel-type structure has been intensively studied in recent years due to their high coercivity and remanence, high coercivity, remanence, magnetocrystalline anisotropy, moderate saturation magnetization, magnetostrictive behavior, and efficient hyperthermia.[3–7] These characteristics make it a candidate system in applications such as magnetic recording, permanent magnets, microwave absorption, and biomedical applications such as drug delivery and magnetic resonance imaging.[8–12] CFO nanoparticles have been synthesized by several techniques, such as sol-gel process, citrate-gel, microemulsions, solid state route, chemical precipitation, and thermal decomposition of organometallic precursors.[13–18] However, these methods are often not simple, and some of them produce undesirable chemical waste. In addition, some methods produce CFO nanoparticles systems with large size distribution and magnetic transitions at low temperatures, indicating the presence of others phases.[13,14] Therefore, the search of a simple and economic route, which allows the preparation of single phase nanocrystalline $CoFe_2O_4$ without the production of chemical residues, is necessary and may increase the applications of this interesting material.

Pulsed laser deposition (PLD) has emerged as a relatively simple, cheap, and highly versatile technique for the growth of nanostructures of a variety of materials including complex oxides directly on substrates.[19,20] Interesting multifunctional materials have been prepared by PLD, including nanopillars of CFO in self-assembled heteroepitaxial nanostructures and thin films.[21–25] However, to our knowledge, no studies on CFO nanoparticles produced by PLD have been published. In this work, we report on the structural and magnetic properties of CFO nanoparticles deposited on the silicon substrate by PLD in the presence of oxygen background. In order to study nanoparticles with different morphologies, the samples were subject to postdeposition heat treatments at 300, 450, and 600 °C. By varying the annealing temperature, the diameter of particles could be controlled between 4.3 and 33.3 nm. The magnetic measurement analysis shows an increase in the blocking temperature from 50 K to beyond room temperature during the annealing process. The nanoparticles exhibit interesting magnetic properties resulting from the evolution of the nanoparticles' nanostructure during annealing.

## II. EXPERIMENTAL PROCEDURE

CFO nanoparticles were deposited on Si substrates by using the PLD system with a Nd:Yag laser ($\lambda = 1064$ nm) with 10 ns pulse duration, 10 Hz repetition rate, and 37 J/cm$^2$. Before deposition, the vacuum chamber was evacuated to $10^{-6}$ Torr, by a turbomolecular pump. For the deposition procedure, $O_2$ gas was introduced into the chamber by a mass flowmeter, in order to achieve 1 Torr pressure. The laser beam was then impinged with 45° incidence angle onto

a)fernandofabris@if.uff.br
b)wnunes@if.uff.br

a commercial $CoFe_2O_4$ commercial target, which was maintained in a 10°/s rotation. The ablation plume expansion in the background is then responsible for the formation of CFO nanoparticles. The nanoparticles were then collected on Si(100) non-heated substrates, which were placed at a distance of 3.3 cm from the target, with 1 h deposition time. After deposition, the samples obtained were annealed in a 1 Torr $O_2$ gas atmosphere, at 300, 450, and 600 °C for 1 h.

X-ray diffraction analysis was performed using a Panalytical XPert PRO diffractometer in the $\theta$–$2\theta$ configuration, with Cu $K_{\alpha 1}$ X-ray. The Raman spectra of the obtained samples were taken in a Witek alpha-300 R confocal Raman microscope, under 532 nm laser irradiation.

Experiments of $^{57}$Fe Mössbauer spectroscopy were done in order to obtain details on the samples' structure. The experiments were performed at room temperature in transmission geometry, with a Co-57 in the Rh-matrix source, moving sinusoidally, also at room temperature. All the isomer shift IS values are obtained relative to metallic iron. The morphology and structure of the CFO nanoparticles were investigated by the transmission electron microscope (TEM, JEOL JEM-2100 F) with 200 keV electron acceleration voltage. For TEM observation, the nanoparticles were removed and suspended in a 10% oleic acid-isopropyl alcohol solution. After sonication, the nanoparticles suspension is dropped over a carbon film covered Cu TEM grid. Magnetic measurements were performed on a Quantum Design VersaLab VSM magnetometer equipped with a 30 kOe magnet in the 50–400 K temperature range. Zero field cooled (ZFC) magnetization curves were measured upon warming with an external field applied after cooling the sample in the zero magnetic field. Field cooled (FC) magnetization curves were measured upon warming under the same applied field used during cooling. Delta-M curves were measured in an alternating gradient magnetometer (Princeton Micromag).

## III. RESULTS AND DISCUSSION

Figure 1 shows the X-ray diffraction related to the as-deposited sample and to the annealed ones. The X-ray diffractograms of the samples annealed at 450 °C and 600 °C show sharp peaks, clearly related to the CFO spinel structure. On the other hand, the diffractograms of the as-deposited and 300 °C-annealed samples show only very broad peaks. In the 300 °C-annealed sample diffractogram, we can see the development of a maximum in the (222) and (400) CFO peak regions. The general behavior of the samples indicates a progressive crystallization as the annealing temperature increases. The lattice parameter of the samples annealed at 450 °C and 600 °C was determined from the diffractogram, and values 8.377 and 8.356Å were obtained, respectively. These values agree well with the lattice parameter obtained by bulk CFO.[26]

Raman spectra of the as-prepared and annealed samples are shown in Fig. 2. The samples exhibit four of the active modes expected by group theory analysis for cubic spinel CFO.[27] All studied samples exhibit a similar Raman spectral profile except for the sample annealed at 300 °C, which shows a pronounced difference between the intensity of peak at around 675 $cm^{-1}$ and 460 $cm^{-1}$. The band around 460 $cm^{-1}$ has been assigned to vibration of oxygen towards $Co^{2+}$ at octahedral sites, whereas the Raman signal near 675 $cm^{-1}$ to the vibration of oxygen towards $Co^{2+}$ and $Fe^{3+}$ at tetrahedral sites. Since the temperature has a significant effect on the $Co^{2+}$ distribution in the lattice of the spinel structure, the changes in the relative Raman intensities observed for the sample annealed at 300 °C would indicate a decrease in $Co^{2+}$ into the octahedral site of the spinel ferrite.[28] This effect can affect the magnetic behavior, since decreasing of $Co^{2+}$ into the octahedral site can increase the moment per molecule of CFO.[15]

The particle size and crystalline structure of the nanoparticles were analyzed by means of transmission electron microscopy (TEM) and selected area electron diffraction (SAED). The results obtained for all samples are shown in Fig. 3. As expected, our CFO nanoparticles are quite agglomerated, as can be seen in low magnification TEM images (left image of each sample in Fig. 3). The as-deposited nanoparticles do not present well-defined shape or clear border. Increasing the annealing temperature, from 300 °C to 600 °C, the particles' growth and a re-arrangement of the atoms occur due to high mobility of these at higher temperatures. The size distribution histogram of each sample is shown in Fig. 3 (up-right). The particle size analysis shows

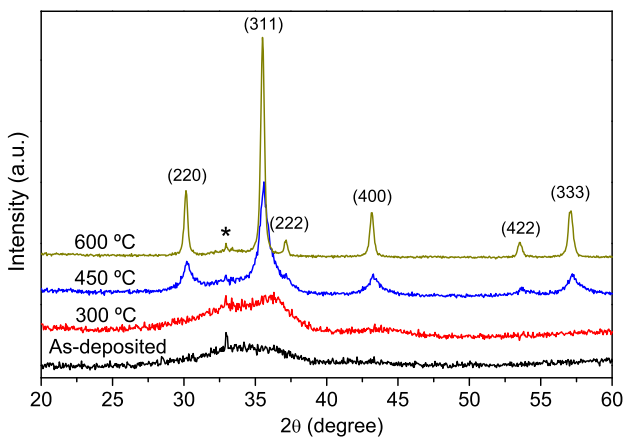


FIG. 1. XRD pattern of CFO samples. The Si substrate peak is marked (*).

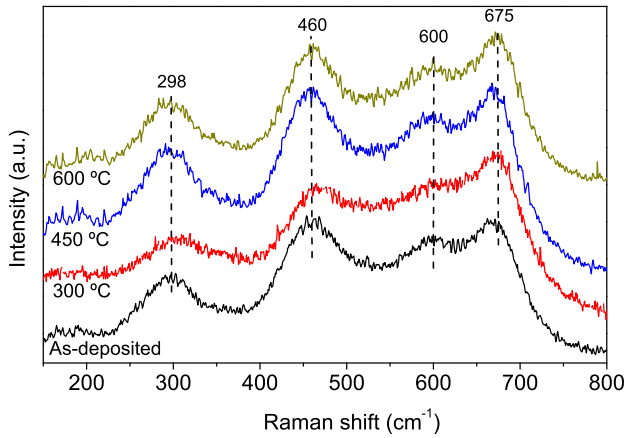


FIG. 2. Raman spectra of the as-deposited and the annealed samples. Numbers indicate the positions of active Raman modes of CFO.

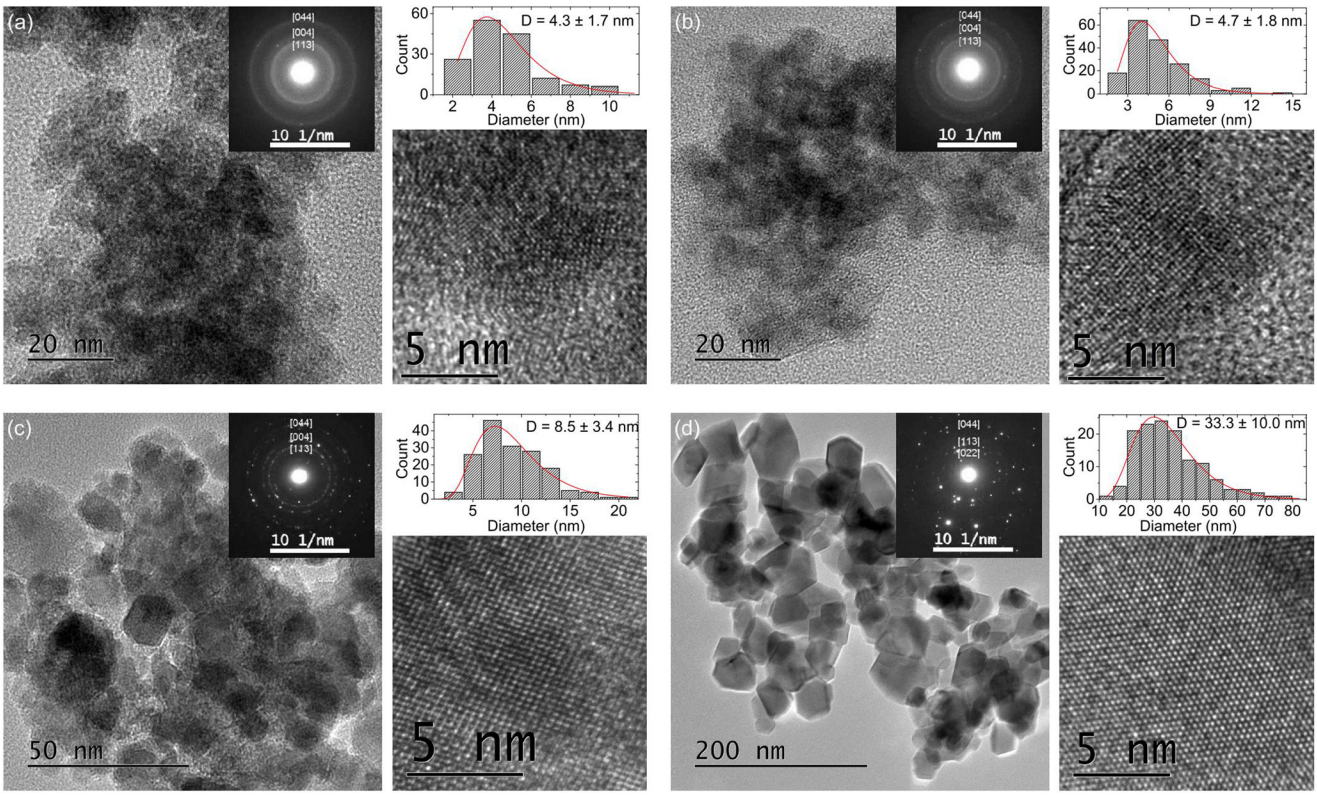


FIG. 3. TEM image (left), SAED pattern (inset left), particle size histogram (top-right), and HRTEM (bottom-right) of sample as-deposited (a), annealed at 300 °C (b), 450 °C (c), and 600 °C (d). Some planes identified in SAED patterns were indexed considering spinel CFO with the Fd3m space group. Red lines are log-normal distributions fitted to the particle size histogram.

a progressive growth of the particle size when the sample is annealed, mainly for the sample annealed at 600 °C. All particle size distributions were fitted using a log-normal distribution, considering the average diameter ($D$) and width of distribution ($\sigma$) as fit parameters. The red lines in Fig. 3 were obtained from the best $D$ and $\sigma$ values shown in Table I. We observed an evolution of the microstructure of the sample as the heat treatment temperature increased. Indeed, the border of the particles becomes clearer, showing regular shapes with regular surfaces corresponding to atomic planes, as seen in SAED patterns (see insets in Fig. 3). The diffraction of the as-prepared sample shows several homogeneous rings with very few bright points, which is a typical character of the nano-crystalline sample with random grain orientation. More bright points are visible in the diffraction pattern of sample annealed at 300 °C, which started breaking the homogeneous rings. For annealed sample at 450 °C, clear points are observed in the diffraction patterns, although weak rings are still present. The sample annealed at 600 °C shows only bright points and the number of crystals in the selected area decreased significantly, indicating the growing and crystallization of the nanoparticles. The diffraction patterns of all samples could be indexed using a cubic structure in the Fd3m space group of spinel CFO. The HRTEM images (bottom-right of each figure) give direct evidence of the above observation. It is possible to observe a grain boundary in a nanoparticle of the as-prepared sample, which suggests that the grain size is smaller than the particle size. Also, the contrast between nanoparticles and amorphous background is quite small, indicating a crystalline structure with a lot of defects. However, the higher was the heat treatment temperature, the better was the contrast observed between the nanoparticles and the background, confirming the crystallization process with annealing.

The Mössbauer spectra (MS) recorded at room temperature are shown in Fig. 4 for all samples. The MS of as-deposited and samples annealed at 300 °C exhibit a doublet, which is typical behavior expected for materials in the paramagnetic or superparamagnetic regime. Since the Curie temperature of $CoFe_2O_4$ bulk is about 520 °C,[29] we attribute the

TABLE I. Mean diameter ($D$) and width of size distribution ($\sigma$, obtained by TEM analysis), coercive fields ($H_C$) at 50 and 300 K and squareness ratio ($M_R/M_S$) at 50 K (obtained of $M$ vs $H$ curves), mean blocking temperature $T_B$ and its width distribution (calculated from $H_C$ vs T curves), and effective magnetic anisotropy constant $K_{eff}$ (calculated using the Néel Model).

| Sample | $D$ (nm) | $H_C$ [50 K] (kOe) | $H_C$ [300 K] (kOe) | $M_R/M_S$ [50 K] | $H_K$ (kOe) | $T_B$ (K) | $K_{eff}$ (erg/cm$^3$) |
|---|---|---|---|---|---|---|---|
| As-deposited | 4.3 ± 1.7 | 2.0 | 0.1 | 0.12 | 17 | 69 ± 9 | $5.7 \times 10^6$ |
| 300 °C | 4.7 ± 1.8 | 3.4 | 0.3 | 0.20 | 22 | 119 ± 15 | $7.6 \times 10^6$ |
| 450 °C | 8.5 ± 3.4 | 13.8 | 0.6 | 0.78 | 74 | 235 ± 33 | $2.5 \times 10^6$ |
| 600 °C | 33.3 ± 10.0 | 12.7 | 1.3 | 0.94 | 65 | 289 ± 41 | $5.1 \times 10^4$ |

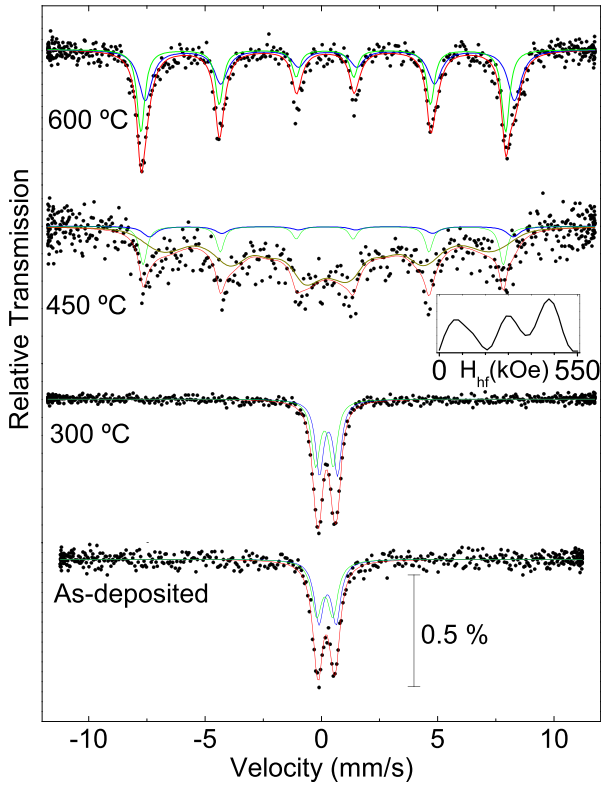


FIG. 4. $^{57}$Fe Mössbauer spectra obtained for all the samples at room temperature. The subspectra corresponding to the tetrahedral (green) and octahedral (blue) sites are shown. The subspectra of the sample annealed at 450 °C have an additional subspectrum corresponding to the magnetic hyperfine field distribution.

Mössbauer doublet observed at room temperature to nanoparticles in the superparamagnetic regime. In fact, X-ray diffraction and electronic microscopy results show average nanoparticle sizes for as-deposited and samples annealed at 300 °C, which are smaller than the critical diameter to form a domain wall in CFO (≈80 nm).[30]

Two doublets were considered in the analysis of the Mössbauer. One doublet was assigned to high-spin $Fe^{3+}$ located in the tetrahedral site A and the other to high-spin $Fe^{3+}$ in the octahedral site B of the $CoFe_2O_4$.[31,32] From the ratio $f_A/f_B$ between the absorption area of the doublets, we can obtain the relative fraction of Co in tetrahedral and octahedral sites for each analyzed sample (see Table II). The ration value taken for the as-deposited sample [0.94(9)] is close to the value 0.94 of the ideal ferrite,[31] indicating that our compound has the same amount of Fe in the octahedral coordination than an ideal ferrite. When the sample is annealed at 300 °C, the ratio decreases slightly (Table II), indicating an increase in the amount of Fe with octahedral coordination and a consequent decrease in the amount of Co with octahedral coordination. Indeed, the decrease of the octahedral sites for the sample annealed at 300 °C is supported by Raman spectroscopy. The linewidth (Γ) of the doublets for sample annealed at 300 °C is smaller compared to the values of the as deposited sample (Table II), indicating a higher crystallinity with the annealing at 300 °C, in agreement with TEM results.

The sample annealed at 450 °C shows a broadened magnetic spectrum. This spectrum was analyzed with two sextets,

TABLE II. Room temperature $^{57}$Fe Mössbauer spectra of the studied samples. Γ is the linewidth and $f_A/f_B$ is the ratio between the absorption areas of the Fe with tetrahedral and octahedral coordination.

| Samples | Fe-sites | Γ (mm/s) | $f_A/f_B$ |
|---|---|---|---|
| As-deposited | Tetr | 0.51(7) | 0.94(9) |
| | Oct | 0.48(6) | |
| 300 °C | Tetr | 0.43(3) | 0.91(5) |
| | Oct | 0.41(2) | |
| 450 °C | Tetr | 0.40(3) | 0.93(9) |
| | Oct | 0.70(5) | |
| | Dist | ⟨0.90⟩[a] | |
| 600 °C | Tetr | 0.40(2) | 0.93(7) |
| | Oct | 0.70(2) | |

[a]The numbers in brackets correspond to the average values of hyperfine parameters of the magnetic distribution.

which we attribute to tetrahedral and octahedral Fe sites in larger blocked particles, plus a magnetic hyperfine distribution which simulate a distribution of particles sizes showing superparamagnetic relaxation. This result agrees with the TEM images showing a broadened distribution of particles sizes centered at 8.5 nm in a size range of 3–20 nm (Fig. 3). From the absorption area of the sextets and hyperfine distribution, we estimated that ∼20% of the particles are blocked and 80% are in the superparamagnetic state with different relaxation times. Joining this result with the TEM images which shows that the majority of the nanoparticles in this compound have sizes less than 8.5 nm, we arrived to blocking temperatures ∼300 K for this sample.

The MS corresponding to the sample annealed at 600 °C shows a well resolved magnetic sextet. The spectrum was analyzed with two sextets attributed to the Fe in tetrahedral and octahedral coordination in a static magnetic field, indicating that the majority of the nanoparticles are blocked at room temperature. The ratio between the tetrahedral and octahedral sites remains the same as that for as-deposited samples.

Figure 5 displays the zero field cooled (ZFC) and field cooled (FC) magnetization curves measured in the plane direction for all samples. Both ZFC and FC magnetization curves of the as-deposited and samples annealed at 300 °C exhibit typical features expected for single-domain nanoparticle systems with irreversibility between ZFC and FC curves below the ZFC maximum.[2] For a superparamagnetic system of noninteracting nanoparticles, the peak of the ZFC curve is strongly related to blocking temperature ($T_B$), below which most part of the nanoparticles are magnetically stable. As can be seen in Fig. 5, $T_B$ increases with annealing at 300 °C, and one can infer that it increases than room temperature for the samples annealed at 450 °C and 600 °C. Furthermore, the decrease of the FC magnetization with decreasing temperature below the ZFC peak observed for samples annealed at 300 °C and 600 °C suggests that the dipolar interactions play an important role in the magnetic properties of these systems.[33]

The low temperature hysteresis loops measured in plane of the as-deposited and the annealed samples are shown in Figs. 6(a) and 6(b). The coercive field ($H_C$) and the squareness ratio ($M_r/M_S$) values obtained at 50 K are reported in

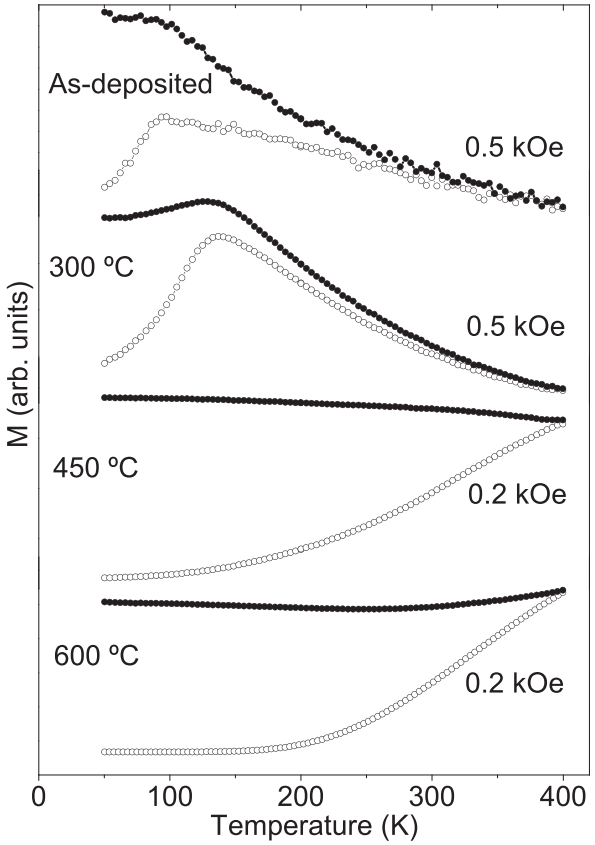


FIG. 5. ZFC (empty circles) and FC (filled circles) magnetization curves as a function of the temperature measured for as-deposited and annealed samples.

Table I. The annealing process produces significant change in the hysteresis loops of the CFO nanoparticles including an enhancement in the coercivity and $M_r/M_s$ ratio values. As shown in Table I, the coercivity of the nanoparticles at 50 K increases from 2 kOe to about 13 kOe, and $M_r/M_S$ increases from 0.1 to 0.9 with the annealing process at or above 450 °C. The values observed for $M_r/M_S$ and coercivity in the present study are in the same range of values of those found for CFO nanoparticles produced by the chemical method.[34] The samples annealed at 450 °C and 600 °C exhibit almost rectangular $M(H)$ loops at 50 K with the squareness ratio well above the value expected from the Stoner and Wohlfarth model for uniaxial anisotropy with easy axis randomly oriented (0.48). The $M_r/M_S$ value for system particles with multiaxial cubic anisotropy was calculated by Walkers *et al.*[35] neglecting interparticle interactions. They found that the $M_r/M_S$ value for temperature below $T_B$ is 0.866 for $K_1 < 0$ and the value 0.831 for $K_1 > 0$. The CFO has cubic magnetocrystalline anisotropy with a very large bulk anisotropy constant ($K_1 = 18.7 \times 10^6$ erg/cm$^3$ at 50 K),[36] and hence, the commonly uniaxial anisotropy contribution as shape and magnetoelastic anisotropy should not have significant influence on effective anisotropy of CFO nanocrystals. On the contrary, according to the random anisotropy model, it is expected that the anisotropy of polycrystalline nanoparticles will be an average over several structural units and, thus, be reduced in magnitude,[37] and consequently, the shape anisotropy can be more relevant than other contribution to

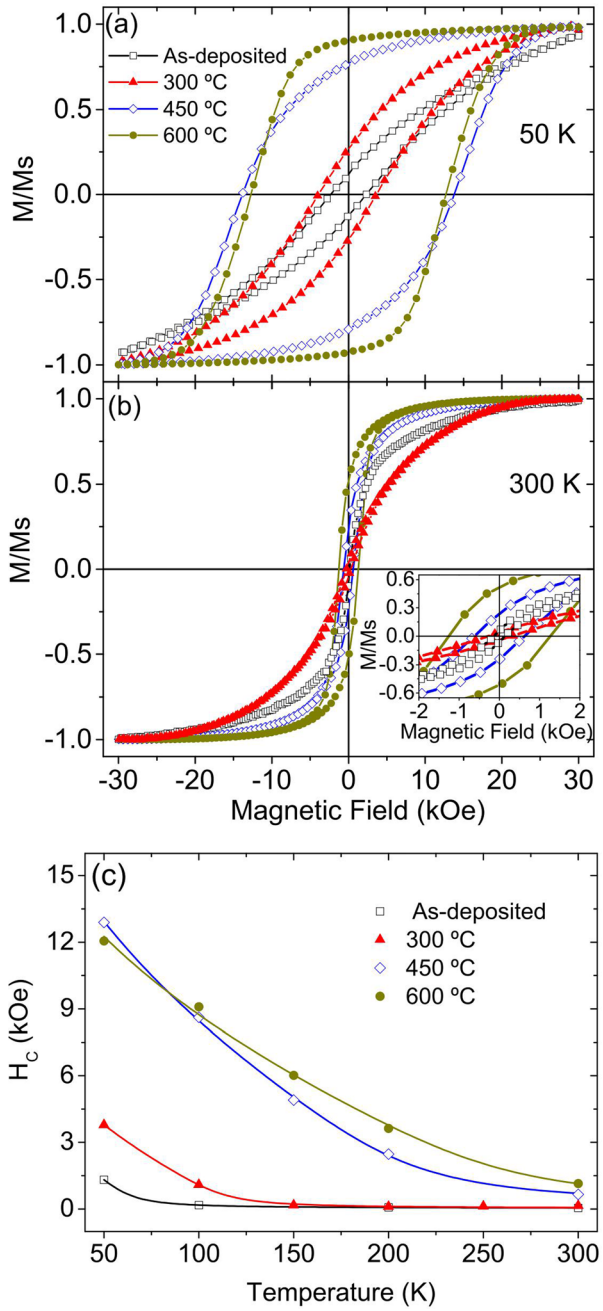


FIG. 6. Normalized moment curves as a function of the field for all samples taken at 50 K (a) and 300 K (b). In (c) the coercive field, $H_C$ versus temperature is plotted for all samples. The inset of (b), we show a zoom of curves measured in 300 K. The solid lines are adjusted considering Eq. (1).

the magnetic anisotropy of polycrystalline CFO nanoparticles. Indeed, $M_r/M_S$ values observed at 50 K for samples having CFO nanocrystals (annealed at 450 °C and 600 °C) are in good agreement with the value expected for CFO cubic nanocrystals (0.831). A fairly larger value for the $M_r/M_S$ value was observed for sample annealed at 600 °C, which we attribute to the interparticle interaction. In contrast, for samples with polycrystalline nanoparticles of CFO (as-deposited and annealed at 300 °C), the $M_r/M_S$ values observed at 50 K were much smaller than the value expected of Stoner and Wohlfarth model (0.48). This last result may be caused by the large number of nanoparticles in superparamagnetic states for these samples at 50 K.

To assess the average $T_B$, the coercive field experimental ($H_c$) data were analyzed according to a non-interacting model.[38] Figure 6(c) shows Hc temperature behavior for as-deposited and annealed samples. The $H_C$ vs $T$ curves were fitted using a distribution of blocking temperature according to the equation[38]

$$H_C = \alpha H_K \left[1 - \left(\frac{T}{\langle T_B \rangle}\right)^{1/2}\right], \quad (1)$$

where $\alpha = 0.48$ for uniaxial anisotropy and $\alpha = 0.32$ for cubic anisotropy,[35,38] $H_K$ is the anisotropy field, and $\langle T_B \rangle$ is the average blocking temperature, which takes into account only the volume fraction of particles that is in blocked state at temperature T. We considered a log-normal distribution of block temperature $f(T_B)$ with the distribution width $\sigma$. The lines in Fig. 6(c) were obtained from the best fit parameter $H_K$, $T_B$, and $\sigma$ (see Table I). The agreement between experimental data and the fitting based on the superparamagnetic framework is quite good, especially considering that neither the nanoparticles are dispersed in a matrix nor their surfaces functionalized. We found a low $T_B$ value of 69 K for the as-deposited sample. In contrast, $T_B$ obtained for the samples annealed at 450 °C and 600 °C are near room temperature. Although Eq. (1) does not consider the interaction between nanoparticles, it can describe the curves of interacting the nanoparticles' systems, but the blocking temperature obtained from this analysis is different from other experimental curves (e.g., ZFC/FC curves).[39]

We can derive a mean value of the effective magnetic anisotropy constant $K_{eff}$ considering that the nanoparticles have uniaxial anisotropy and the time of measurement of about 100 s; thus, $K_{eff}V = 25k_BT_B$, $T_B$ obtained by the $H_C$ curves fitting, and the average particle size of TEM analysis. The obtained $K_{eff}$ values are shown in Table I. As bulk crystal of CFO has cubic anisotropy with magnetocrystalline anisotropy constant $K_1 > 0$, the comparison of $K_{eff}$ with $K_1$ is given by the relation $K_{eff} = K_1/4$;[40] hence, at 300 K, the bulk $K_{eff} \sim 1.0 \times 10^6$ erg/cm$^3$.[36] The $K_{eff}$ values obtained for samples annealed at and below 450 °C are fairly larger than the bulk value, whereas it is much smaller for sample annealed at 600 °C. The properties of magnetic nanoparticles are not the same as those of bulk materials, and many experiments have shown an increase of the effective magnetic anisotropy due to the surface anisotropy.[41] The exceptions are systems with very strong interparticle interactions where, according with some authors, the magnetic properties provide information not of individual nanoparticles but of group of nanoparticles with very small effective magnetic anisotropy.[42] Thus, the very low value of $K_{eff}$ obtained for the sample annealed at 600 °C can be claimed to the influence of interparticle interactions.

The interactions among nanoparticles were further investigated by using the $\Delta M$ technique (also known as the Henkel plot).[43] This formalism is based on the comparison of the isothermal remanent magnetization ($M_{IRM}$) and dc-demagnetization ($M_{DcD}$) curves. Both $M_{IRM}$ and $M_{DcD}$ are remanence curves that depend on the switching field distribution in the system. However, although the $M_{IRM}$ curve is taken from an initial state in which the nanoparticles have randomly oriented moments, $M_{DcD}$ is taken from an initial state in which the magnetic moments are aligned. The $\Delta M$ is calculated from these two curves,

$$\Delta M = \frac{M_{DcD}(H)}{M_{IRM}(\infty)} - \left(1 - 2\frac{M_{IRM}(H)}{M_{IRM}(\infty)}\right). \quad (2)$$

Effectively $\Delta M$ gives the difference between the fractions of magnetic moments switched by the applied field in $M_{IRM}$ and $M_{DcD}$ modes. As the effect of interaction depends on the moment configuration, the $\Delta M(H)$ curve can provide relevant information about the nature and strength of such interactions, for instance, for a noninteracting system one expects $\Delta M = 0$.[43] Fig. 7 (inset) shows typical room temperature $\Delta M$ curves for the as-deposited sample calculated from $M_{IRM}(H)$ and $M_{DcD}(H)$ curves. Similar curves were obtained for other samples. For all samples, the $\Delta M$ curves display negative peaks suggesting that the interparticle interaction is dominated by the magnetostatic interaction. The negative peak is more pronounced for annealed at 300 °C and 600 °C samples indicating that these samples have higher interaction strength. In fact, FC curves of these samples show a bump at low temperature that corroborates with a demagnetizing interaction among nanoparticles; see Fig. 5. The origin of high interaction strength observed for annealing at 600 °C may be related to the increase of nanocrystals size and, consequently, their magnetic moment with the annealing. The origin of this increases observed for sample annealed at 300 °C is more complex, because these nanoparticles have nearly the same size and the effective anisotropy value of the as-deposited sample that has lower interaction effects on its magnetic properties. This effect observed for sample annealed at 300 °C may be related to the increase of the effective magnetic moments of the $CoFe_2O_4$ nanoparticles with the diffusion of the $Co^{2+}$ ions from octahedral to tetrahedral sites, as observed in the Raman and Mössbauer analyses.

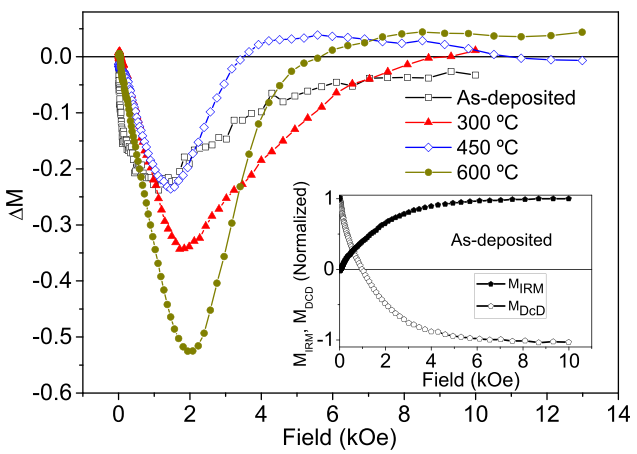


FIG. 7. $\Delta M$ curves measured in 300 K for the as-deposited sample, annealed at 300 °C, annealed at 450 °C, and annealed at 600 °C. The inset shows the normalized isothermal remnant magnetization $M_{IRM}(H)$ and the demagnetizing remanence $M_{DcD}(H)$ of the as-deposited sample.

A carefully analysis of $\Delta M$ curves obtained for samples annealed at 450 °C and 600 °C shows the positive $\Delta M$ value for high applied field values, which suggests that interparticle interactions in these samples also support the magnetized state. Although the magnetic properties of sample annealed at 450 °C are affected by the interparticle interaction, it is not stronger enough to couple group of nanoparticles. On the other hand, the annealing at 600 °C promotes a significantly decrease in the effective anisotropy constant as well as an increase of the nanoparticles average size and the magnetic interaction.

## IV. CONCLUSION

In conclusion, we have deposited nanoparticles of $CoFe_2O_4$ with spinel phase directly on the Si substrate by a relatively simple and highly versatile technique, the pulsed laser deposition. With post annealing up to 600 °C, it was possible to change the size, crystallinity, and coercivity of the nanoparticles, which will be useful in investigations of magnetically interacting nanostructure, as well as for permanent magnetic devices based on nanoparticles. We found that the magnetization properties of the CFO nanoparticles can be dominated by cubic magnetocrystalline or a uniaxial effective anisotropy depending on the annealing temperature.

## ACKNOWLEDGMENTS

This work was supported by Brazilian Agencies CNPq, CAPES, and FAPERJ. W.C.N. is grateful to Caroline A. Ross and Suchi Ojha for assistance in PLD and thoughtful discussion, and Eduardo Martin for assistance in AGM.

[1]A. G. Kolhatkar, A. C. Jamison, D. Litvinov, R. C. Willson, and T. R. Lee, Int. J. Mol. Sci. **14**, 15977 (2013).
[2]M. Knobel, W. Nunes, L. Socolovsky, E. De Biasi, J. Vargas, and J. C. Denardin, J. Nanosci. Nanotechnol. **8**, 2836 (2008).
[3]A. Franco, F. L. A. Machado, and V. S. Zapf, J. Appl. Phys. **110**, 053913 (2011).
[4]A. Muhammad, R. Sato-Turtelli, M. Kriegisch, R. Grössinger, F. Kubel, and T. Konegger, J. Appl. Phys. **111**, 013918 (2012).
[5]S. Goh, C. Chia, S. Zakaria, M. Yusoff, C. Haw, S. Ahmadi, N. Huang, and H. Lim, Mater. Chem. Phys. **120**, 31 (2010).
[6]T. E. Torres, A. G. Roca, M. P. Morales, A. Ibarra, C. Marquina, M. R. Ibarra, and G. F. Goya, J. Phys.: Conf. Ser. **200**, 072101 (2010).
[7]I. Sharifi, H. Shokrollahi, and S. Amiri, J. Magn. Magn. Mater. **324**, 903 (2012).
[8]N. Sanpo, C. Wen, C. C. Berndt, and J. Wang, "Multifunctional spinel ferrite nanoparticles for biomedical application," in *Advanced Functional Materials* (John Wiley and Sons, Inc., 2015), pp. 183–217.
[9]L. Xi, Z. Wang, Y. Zuo, and X. Shi, Nanotechnology **22**, 045707 (2011).
[10]M. Colombo, S. Carregal-Romero, M. F. Casula, L. Gutierrez, M. P. Morales, I. B. Bohm, J. T. Heverhagen, D. Prosperi, and W. J. Parak, Chem. Soc. Rev. **41**, 4306 (2012).
[11]S. Singamaneni, V. N. Bliznyuk, C. Binek, and E. Y. Tsymbal, J. Mater. Chem. **21**, 16819 (2011).
[12]A. H. Habib, C. L. Ondeck, P. Chaudhary, M. R. Bockstaller, and M. E. McHenry, J. Appl. Phys. **103**, 07A307 (2008).
[13]F. Zeb, W. Sarwer, K. Nadeem, M. Kamran, M. Mumtaz, H. Krenn, and I. Letofsky-Papst, J. Magn. Magn. Mater. **407**, 241 (2016).
[14]R. S. Turtelli, G. V. Duong, W. Nunes, R. Grössinger, and M. Knobel, J. Magn. Magn. Mater. **320**, e339 (2008).
[15]D. S. Mathew and R.-S. Juang, Chen. Eng. J. **129**, 51 (2007).
[16]A. C. H. Barreto, V. R. Santiago, R. M. Freire, S. E. Mazzetto, J. M. Sasaki, I. F. Vasconcelos, J. C. Denardin, G. Mele, L. Carbone, and P. B. A. Fechine, J. Mater. Eng. Perform. **22**, 2073 (2013).
[17]Z. Jiao, X. Geng, M. Wu, Y. Jiang, and B. Zhao, Colloids Surf. A: Physicochem. Eng. Aspects **313**, 31 (2008).
[18]C. Cannas, A. Musinu, A. Ardu, F. Orru, D. Peddis, M. Casu, R. Sanna, F. Angius, G. Diaz, and G. Piccaluga, Chem. Mater. **22**, 3353 (2010).
[19]C. V. Cojocaru, C. Harnagea, F. Rosei, A. Pignolet, M. A. F. van den Boogaart, and J. Brugger, Appl. Phys. Lett. **86**, 183107 (2005).
[20]H. M. Christen and G. Eres, J. Phys. Condens. Matter. **20**, 264005 (2008).
[21]P. C. Dorsey, P. Lubitz, D. B. Chrisey, and J. S. Horwitz, J. Appl. Phys. **79**, 6338 (1996).
[22]P. Thang, G. Rijnders, and D. Blank, J. Magn. Magn. Mater. **310**, 2621 (2007).
[23]A. Jha, N. Kumar, S. Chaubey, and M. Sahni, J. Supercond. Nov. Magn. **29**, 855 (2016).
[24]H. Zheng, J. Wang, S. E. Lofland, Z. Ma, L. Mohaddes-Ardabili, T. Zhao, L. Salamanca-Riba, S. R. Shinde, S. B. Ogale, F. Bai, D. Viehland, Y. Jia, D. G. Schlom, M. Wuttig, A. Roytburd, and R. Ramesh, Science **303**, 661 (2004).
[25]H.-J. Liu, Y.-Y. Liu, C.-Y. Tsai, S.-C. Liao, Y.-J. Chen, H.-J. Lin, C.-H. Lai, W.-F. Hsieh, J.-Y. Li, C.-T. Chen, Q. He, and Y.-H. Chu, Sci. Rep. **5**, 12073 (2015).
[26]S. Imine, F. Schoenstein, S. Mercone, M. Zaghrioui, N. Bettahar, and N. Jouini, J. Eur. Ceram. Soc. **31**, 2943 (2011).
[27]W. Chen and W. Zhu, J. Am. Ceram. Soc. **94**, 1096 (2011).
[28]G. Shemer, E. Tirosh, T. Livneh, and G. Markovich, J. Phys. Chem. C **111**, 14334 (2007).
[29]R. A. McCurrie, *Ferromagnetic Materials- Structure and Properties* (Academic Press, 1994).
[30]L. Zhao, H. Zhang, Y. Xing, S. Song, S. Yu, W. Shi, X. Guo, J. Yang, Y. Lei, and F. Cao, J. Solid. State. Chem. **181**, 245 (2008).
[31]G. A. Sawatzky, F. Van Der Woude, and A. H. Morrish, Phys. Rev. **183**, 383 (1969).
[32]A. Lima, M. Morales, J. Araújo, J. Soares, D. Melo, and A. Carriço, Ceram. Int. **41**, 11804 (2015).
[33]W. Nunes, A. Gomes, R. Rapp, and M. Novak, J. Magn. Magn. Mater. **370**, 116 (2014).
[34]A. López-Ortega, E. Lottini, C. d J. Fernández, and C. Sangregorio, Chem. Mater. **27**, 4048 (2015).
[35]M. Walker, P. I. Mayo, K. O'Grady, S. W. Charles, and R. W. Chantrell, J. Phys. Condens. Matter **5**, 2779 (1993).
[36]H. Shenker, Phys. Rev. **107**, 1246 (1957).
[37]G. Herzer, Scr. Metall Mater. **33**, 1741 (1995).
[38]W. C. Nunes, W. S. D. Folly, J. P. Sinnecker, and M. A. Novak, Phys. Rev. B **70**, 014419 (2004).
[39]W. C. Nunes, F. Cebollada, M. Knobel, and D. Zanchet, J. Appl. Phys. **99**, 08N705 (2006).
[40]J. L. Dormann, D. Fiorani, and E. Tronc, "Magnetic relaxation in fine-particle systems," in *Advances in Chemical Physics* (John Wiley and Sons, Inc., 2007), pp. 283–494.
[41]M. Respaud, J. M. Broto, H. Rakoto, A. R. Fert, L. Thomas, B. Barbara, M. Verelst, E. Snoeck, P. Lecante, A. Mosset, J. Osuna, T. O. Ely, C. Amiens, and B. Chaudret, Phys. Rev. B **57**, 2925 (1998).
[42]J. M. Vargas, W. C. Nunes, L. M. Socolovsky, M. Knobel, and D. Zanchet, Phys. Rev. B **72**, 184428 (2005).
[43]P. E. Kelly, K. O'Grady, P. I. Mayo, and R. W. Chantrell, IEEE Trans. Mag. **25**, 3881 (1989).